JOURNAL OF PETROLOGY | VOLUME 47 | NUMBER 3 | PAGES 631–646 | 2006 | doi:10.1093/petrology/egi090

Mantle Mush Compaction: a Key to Understand the Mechanisms of Concentration of Kimberlite Melts and Initiation of Swarms of Kimberlite Dykes

M. GRÉGOIRE[1]*, M. RABINOWICZ[1] AND A. J. A. JANSE[2]

[1]LABORATOIRE DE DYNAMIQUES TERRESTRE ET PLANÉTAIRE-CNRS UMR 5562, OBSERVATOIRE MIDI-PYRÉNÉES, UNIVERSITÉ PAUL SABATIER, 14 AVENUE E. BELIN, 31400 TOULOUSE, FRANCE

[2]ARCHON EXPLORATION PTY LTD, 11 ROSLEY WAY, CARINE, PERTH, W.A. 6020, AUSTRALIA

RECEIVED MAY 9, 2005; ACCEPTED NOVEMBER 3, 2005
ADVANCE ACCESS PUBLICATION DECEMBER 8, 2005

Kimberlite pipes or dykes tend to occur in clusters (a few kilometres in diameter) within fields ~30–50 km in diameter. They are generally considered to originate from low degrees of partial melting of carbonated peridotite within zones of ascending mantle. Numerical modelling shows that at the depth of formation of kimberlite melts (≫200 km), mantle compaction processes can result in the formation of melt pockets a few tens of kilometres across, with melt concentrations up to 7%. The initiation of swarms of kimberlite dykes at the top of these melt pockets is inevitable because of the large excess pressure between the melt and the surrounding solid, which exceeds the hydraulic fracturing limit of the overlying rocks. After their initiation at mantle depth the swarm of dykes may reach the surface of the Earth when the entire cratonic lithosphere column is in extension. We propose that kimberlite fields represent the surface envelope of dyke swarms generated inside a melt pocket and that kimberlite clusters represent the discharge of melt via dykes originating from sub-regions of the pocket. This model reproduces the worldwide average diameter of kimberlite fields and is consistent with the observation that some of the main kimberlite fields display age ranges of c. *10 Myr. It is deduced that, at the scale of the Kaapvaal craton, different fields such as Kimberley, N. Lesotho and Orapa, dated at 80–90 Ma, probably result from synchronous melt pockets forming inside an ascending mantle flow. The same model could apply to the fields of the Rietfontein, Central Cape and Gibeon districts dated at 60–70 Ma. It is suggested that the same mantle flow that produced the Kimberley, N. Lesotho and Orapa fields migrated over ~20–30 Myr a few hundred kilometres westward to form the Rietfontein, Central Cape and Gibeon fields.*

KEY WORDS: *kimberlites; mantle; compaction; convection; volcanism*

INTRODUCTION

Main features of kimberlitic melts and type of occurrences

Kimberlites are potassic ultrabasic igneous rocks, which have been subdivided into Group 1 and Group 2 types (Le Maitre, 2002). Both groups are volatile-rich (Group I is CO_2 dominant, and Group II is H_2O dominant; Smith *et al.*, 1985; Skinner, 1989; Mitchell, 1995). Kimberlites are restricted in occurrence to cratons and their margins, and are of great geological interest because: (1) they offer a direct window into the nature and evolution of the sub-continental cratonic lithospheric mantle at depths in excess of 150 km, by transporting xenoliths and xenocrysts to the surface of the Earth (e.g. Nixon, 1987; Gurney *et al.*, 1991); (2) kimberlitic melts are important metasomatic agents leading to textural, mineralogical and geochemical modifications of the lithospheric mantle (e.g. Erlank *et al.*, 1987; Van Achterbergh *et al.*, 2001; Grégoire *et al.*, 2002, 2003); (3) they often contain diamonds and are the host rock of most economic diamond deposits (e.g. Harris, 1992).

Numerous petrological, geochemical and isotopic studies have linked kimberlites to the activity of thermally anomalous mantle plumes (e.g. Le Roex, 1986; Haggerty, 1994); however, others have invoked diapiric

*Corresponding author. Telephone: +33 5 61332977. Fax: +33 5 61332900. E-mail: Michel.Gregoire@dtp.obs-mip.fr

or subduction processes (Green & Guegen, 1974; Helmstaedt & Gurney, 1997). Nevertheless, there seems to be a consensus that kimberlitic melts represent very low degrees (<1%) of partial melting of carbonated lherzolitic mantle sources in the deep part of the upper mantle located between the base of the cratonic lithosphere and the top of the lower mantle (e.g. Canil & Scarfe, 1990; Ringwood *et al.*, 1992; Dalton & Presnall, 1998).

In the upper mantle, the density contrast $\delta\rho$ between kimberlitic melt (~2400–2500 kg/m^3) and the mantle rocks (~3300–3400 kg/m^3) is about 1000 kg/m^3, i.e. twice the contrast between basaltic melt and mantle rocks at low pressure (Spera, 1984; McKenzie, 1985; Scarfe *et al.*, 1987). There is no evidence that the kimberlitic melts, probably because they are volatile-rich, could become more dense than the olivine- and pyroxene-rich host mantle at pressures of 6–10 GPa such as proposed for volatile-poor basaltic magmas (Stolper *et al.*, 1980; Ridgen *et al.*, 1984).

Kimberlitic melts are efficient metasomatic agents as a result of their low dihedral wetting angles when they are in contact with olivine (25–30°). They strongly react with their mantle peridotite wall rocks causing dissolution of garnet and orthopyroxene and precipitation of new mineral phases such as phlogopite, amphibole and oxides (e.g. Erlank *et al.*, 1987; Van Achterbergh *et al.*, 2001; Grégoire *et al.*, 2002, 2003). The evidence for such reactions mostly comes from studies of mantle xenolith samples equilibrated within the lithospheric cratonic roots (depths shallower than 200–250 km). It is likely that similar reactions also occur in the deeper part of the upper mantle (to 410 km depth) and in the Transition Zone (410–660 km; reaction with ringwoodite, wadsleyite and majoritic garnet).

Kimberlites and related melts often exhume xenoliths of mantle material, which represents the cratonic lithospheric roots beneath kimberlite fields (e.g. Gurney *et al.*, 1991; Pearson *et al.*, 2003). Among these mantle xenoliths is a group that consists of deformed high-T garnet peridotites (e.g. Gurney *et al.*, 1991; Pearson *et al.*, 2003). These occur in numerous kimberlite localities worldwide and are commonly the deepest xenoliths observed (equilibration pressures generally from 4·5 to >6·5 GPa). They display evidence of mantle–melt reactions (e.g. Grégoire *et al.*, 2003). Their textures are porphyroclastic and mosaic-porphyroclastic with fine neoblasts of olivine (<1 mm).

Kimberlites show two main types of occurrence: pipes and dykes. Kimberlite pipes rarely exceed 1 km in diameter, whereas dykes are typically 0·5–3 m wide and can sometimes be followed for several kilometres (Garanin *et al.*, 1993; Basson & Viola, 2003). Pipes are only a superficial feature of the kimberlitic activity and their roots are dykes (e.g. Janse, 1984; Garanin *et al.*, 1993; Basson & Viola, 2003). The distribution of kimberlite pipes and dykes is characterized by clusters, fields, districts and provinces. Clusters are of the order of 5–10 km across, fields a few tens of kilometres (typically 30–50 km), districts a few hundred kilometres and provinces are measured in thousands of kilometres (Janse, 1984; Garanin *et al.*, 1993; Basson & Viola, 2003). Most available radiometric dates on kimberlites are from the 1980s, and hence have relatively large errors; typically all the kimberlites in a cluster and a field have similar ages of intrusion within analytical uncertainties. Nevertheless, in one of the most intensely studied cratonic areas, the Kaapvaal craton, South Africa, the main fields display an age range of *c.* 10 Myr (e.g. Allsopp & Barrett, 1975; Kramers *et al.*, 1983; Smith *et al.*, 1985; Allsopp *et al.*, 1989; Basson & Viola, 2003). Districts and especially provinces frequently include a range of kimberlitic occurrences of different intrusion ages (Garanin *et al.*, 1993). Different kimberlite fields and sometimes districts separated by a few tens of kilometres to several hundred kilometres may display similar intrusion ages. As an example, the group of five economic kimberlites around the town of Kimberley in South Africa define a cluster with a diameter of 8 km and an age around 85 Ma (analytical error on the age of each locality ranges from 1 to 3 Ma). This is one cluster within a field 40 km in diameter, containing at least 20 kimberlite clusters with ages ranging from 80 to 90 Ma (analytical error on age of each dyke and pipe ranges from 1 to 3 Ma). This field lies, in turn, within the Kimberley district, with dimensions of at least 200 km × 100 km and kimberlite ages ranging from 80 to 120 Ma (Fig. 1); this forms part of the on-craton Kaapvaal kimberlite province (Fig. 2).

The processes involved in the intrusion of kimberlite dykes within the lithosphere are relatively well understood (Spera, 1984; White *et al.*, 1995; Lorenz *et al.*, 1999; Sleep, 2003). The propagation of these dykes within the lithosphere has been shown to be rapid (Spera, 1987); simple crack-propagation models suggest that it takes about 14 h for a kimberlitic dyke to travel from a depth of 150 km to the surface; the maximum width at the base of the crack is ~3 m.

Goals of the present study

Several important questions related to the genesis of kimberlite pipes and dykes are not fully understood: (1) What kind of processes generate the excess magma pressure necessary to initiate dyke propagation at mantle depths and kimberlite diatreme formation? (2) Why do the pipes and dykes of a single cluster such as the Kimberley cluster (probably the most dated) fall within the same ~10 Myr age interval? (3) Why do kimberlite clusters display a characteristic size of several kilometres? (4) Why are clusters of similar age distributed in fields with typical diameters of a few tens of kilometres? (5) Why

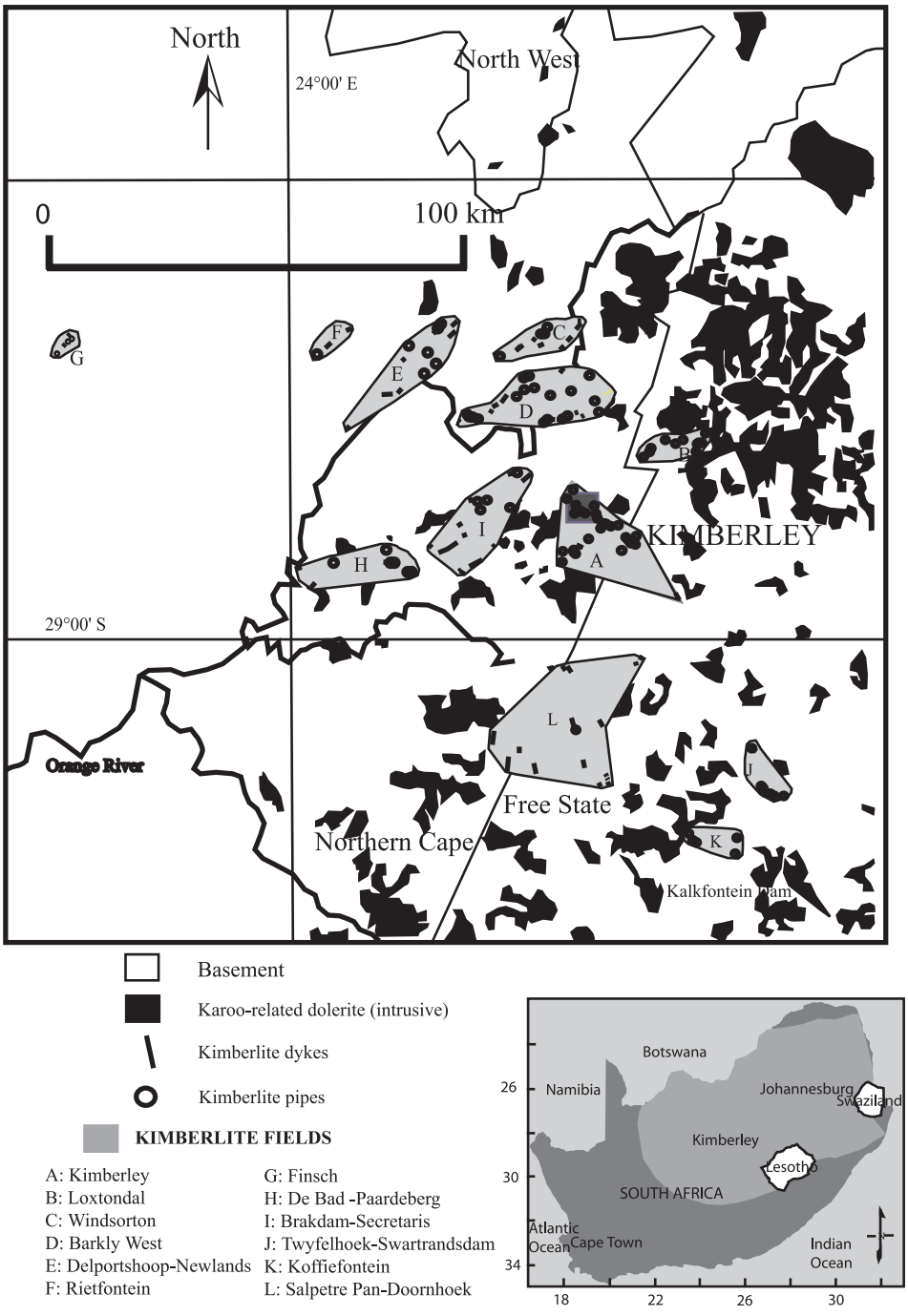

Fig. 1. Geological sketch map of the Kimberley district (South Africa) displaying the location of its kimberlite fields.

are kimberlite fields grouped in large districts a few hundred kilometres across?

The goal of this study is to show that answers to the above questions are linked to melt redistribution and migration at depths exceeding several hundred kilometres. We propose that the driving force for melt migration is the buoyancy of the melt resulting from the density contrast between the kimberlite melt and the mantle wall-rock, $\delta\rho$. In this model we propose that the compaction of the residual peridotite–kimberlite melt mush triggers the formation of swarms of kimberlite dykes at depth.

We start with an overview of what it is known about the generation of dykes from zones of partially molten mantle, and then present the adopted set of equations

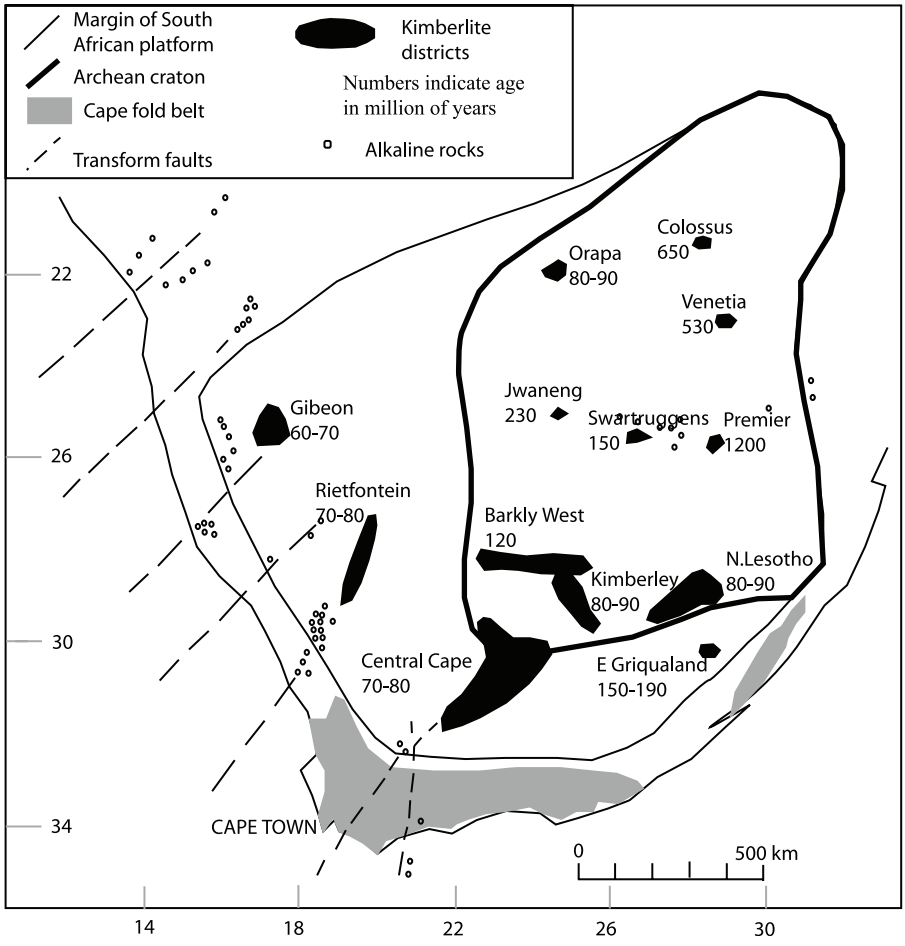

Fig. 2. Distribution and localization of the main kimberlite districts in the South African kimberlite province [modified after Garanin *et al.* (1993)]. The ages indicated are those of the main fields in each district.

and the Equation of State for compaction. The equations are then made dimensionless and the parameters of the model are fixed. We then show the results of the model, which allow estimation of the time of generation of the kimberlite melt pockets, and their sizes. Special attention is paid to the evolution of the excess melt pressure in the mush during the transient development of these pockets. We discuss how and when kimberlite dykes are generated in the compacting mush. We finally show how the results of the model can be used to account for the distribution patterns and origin of kimberlite pipes and dykes outlined above.

GENERATION OF DYKES FROM ZONES OF PARTIALLY MOLTEN MANTLE

The formation of veins or dykes can within the mantle result from (1) melt chanelling (Stevenson, 1989), (2) melt infiltration (Spiegelman & Kelemen, 2003), or (3) magma-fracturing (Spera, 1987; Rubin, 1995). The propagation of veins by magma-fracturing occurs when the excess pressure of the melt (σ_c) in the veins exceeds the tensile strength of the wall-rocks (Spera, 1987; Rubin, 1995). The excess pressure corresponds to the pressure differential between the melt and the residual solid in the partially molten mantle mush. Estimates of the critical excess pressure of the melt for a dyke whose tip is melt free range from 40 to 50 MPa (Spera, 1987). In this case the dyke thickness (Δl) is related to its height (l) by

$$\Delta l = \frac{\sigma_c}{M} l \qquad (1)$$

where $M \sim 50$ GPa designates the elastic stiffness of the mantle (Rubin, 1995). (All the symbols used in equations are defined in Table 1.) In this case dykes of 1 m thickness and 1 km height can easily develop. They propagate at a velocity that is related to the pressure drop owing to the shear stress induced by the magma

Table 1: Explanation of the symbols used in the various equations

$\vec{\nabla}$	Gradient (mathematical function)
p and p_{sc} and p'	Excess pressure
$\delta\rho$	Density contrast between solid and liquid
η	Shear or plastic viscosity
ζ	Bulk viscosity
ϕ and ϕ_{sc} and ϕ'	Melt concentration
t and t_{sc} and t'	Time
g	Gravity constant
z and z'	Vertical coordinate
μ	Magma viscosity
$k(\phi)$ and $k(\phi_{sc})$	Effective permeability
n	Dimensionless constant
a	Characteristic size of the solid grains
L	Compaction length

Prime and subscript sc denote dimensionless and scaled values, respectively.

flowing along the dyke walls (Spera, 1987). Because of the relative large width of the dykes and the low viscosity of the kimberlite melts this stress is negligible and thus the ascent velocity is constrained by the velocity of sound in the solid (Spera, 1987). Much lower values of the excess pressure of the melt have been estimated in the case of veins propagating in a crystal mush with a high intergranular melt content, close to 1 MPa (Rubin, 1998). Finger-like melt veins result from the development of a hydrodynamic instability caused by the buoyancy of the melt in a poro-elastic mush (Rubin, 1998). In this case the dykes are only millimetres in thickness and kilometres in height. Consequently, the propagating ascent velocity of melt in these thin dykes is reduced relative to that in the thick dykes by a factor proportional to the square of the dyke thickness (Rubin, 1998). Thus they cannot explain how the kimberlite dykes can cross the whole lithospheric mantle in less than 1 day and entrain deep mantle xenoliths up to 1 m in size.

THE EQUATIONS OF THE MODEL

The pressure equation

The excess pressure (p in this study), which represents the difference in pressure between the melt and the surrounding solid in a partially molten crystal mush, does not depend only on the density contrast $\delta\rho$ between the solid and the melt. In fact, the pressure drop is related to the intergranular melt flow, which reduces the growth of the excess pressure. As a result, a correct estimation of p in a partially, molten, plastic mantle requires explicit resolution of the compaction equations. During the 1980s equations describing the coupled evolution of the solid-state plastic and melt flow in the mantle were proposed (Sleep, 1974; McKenzie, 1984; Scott & Stevenson, 1986). The most popular model was formulated by McKenzie (1984), who assumed that (1) the pressure in the solid and liquid fractions of the mush are the same and (2) the mush is deformable and compressible. In this case, its rheology depends on two viscosities: a shear viscosity (η) and a bulk viscosity (ζ). The excess pressure p in McKenzie's formalism is zero ($p = 0$) and thus cannot be deduced from the two-phase (melt + solid) equations. Scott & Stevenson (1986) proposed that the excess pressure field p could be related to $\mathrm{d}\phi/\mathrm{d}t$, i.e. the rate of variation of the melt concentration ϕ in the mush with time t. In their model ϕ, η and p are related by the following equation:

$$p = \frac{\eta}{\phi}\frac{\mathrm{d}\phi}{\mathrm{d}t}. \qquad (2)$$

This equation was found to be exact in the case of water flow inside a partially molten icecap (Fowler, 1984). Bercovici *et al.* (2001) recently developed a new formalism to describe two-phase flow. Their formalism assumes: (1) an incompressible mush with a plastic viscosity η representing that of the melt-free solid fraction of the mush, (2) an equation of state relating the excess pressure p to melt concentration ϕ similar to that used by Scott & Stevenson (1984) [equation (2) above]. Actually, the formalism developed by Bercovici *et al.* (2001) generalizes that developed by McKenzie (1984). When the melt concentration is very small and the bulk viscosity ζ is equal to η/ϕ, both formalisms (McKenzie, 1984; Bercovici *et al.*, 2001) lead to the same equation for the evolution of the melt proportion ϕ during compaction. However, only the formalism of Bercovici *et al.* (2001) allows computation of the excess pressure field p during compaction. The knowledge of this field is important, as shown here, because it allows us to understand how kimberlite dykes can be triggered in the sub-cratonic mantle.

The equation of conservation of stresses per unit volume

The buoyancy of melt and temperature gradients drive convection, diapiric flow and compaction within the plastic domain of the upper mantle. It is currently accepted that below cratonic domains the mantle flow of convective plumes, shear zones related to plate-drift, and diapirs related to melting are 50–200 km in size (Van Thienen *et al.*, 2003). These flows have a weak impact on mantle compaction (Scott & Stevenson, 1986). As a result, in our model we assume that the plastic mantle flow pushes the mush upward at an uniform velocity of a few centimetres per year. Rearrangement of the Bercovici *et al.* (2001) equations leads to the following scalar stress conservation

equation (see Rabinowicz *et al.*, 2002):

$$\vec{\nabla}(k(\phi)\,.\,\vec{\nabla}_p) - \frac{\phi}{\mu}p = \delta\rho g\frac{\partial(k(\phi))}{\partial z} \qquad (3)$$

where g, z, μ and $k(\phi)$ represent the acceleration due to gravity, the vertical coordinate, the magma viscosity and the effective permeability of the mush, respectively. Equation (3) assumes that: (1) the geometrical reference frame moves as the same speed as the uniform upward mantle flow, (2) the melt concentration is small and (3) the surface tension between melt and solid is negligible. In equation (3) the term on the right-hand side represents buoyancy. The first term on the left-hand side represents the stress per unit volume caused by deformation of the solid fraction by compaction or dilatation of the mush, and the second term represents the friction of the melt flow within the porosity network (Ribe, 1985; Sparks & Parmentier, 1991).

The permeability equation

Compaction starts when the intergranular melt forms a connected network. Studies of mantle xenoliths entrained in alkaline basalts and kimberlites provide convincing evidence for the circulation of carbonatitic and carbonated highly alkaline mafic silicate melts in the upper mantle (Green & Wallace, 1988; Dautria *et al.*, 1992; Griffin *et al.*, 1992; Rudnick *et al.*, 1993; Sweeney *et al.*, 1993; Chalot-Prat & Boullier, 1997; Ionov, 1998; Yaxley *et al.*, 1998; Grégoire *et al.*, 2000). Static experimental studies show that such melts, in contact with olivine, have low dihedral wetting angles (25–30°, Hunter & McKenzie, 1989; Watson *et al.*, 1990). These low angles imply that very thin films of melt (possibly as low as a few hundred ångströms) wet or partly wet grain boundaries and penetrate along grain edges to form an interconnected network of melt tubes with roughly triangular cross-sections (Hess, 1994). Furthermore, the variation of volume as a result of melting provides transient viscoelastic stresses likely to result in the generation of interconnected cracks filled with melt (Maaløe, 2003). Experiments performed to investigate the interconnectivity of carbonate melt in a dunite suggest that the mantle is permeable for any local melt concentration ϕ exceeding about 10^{-5}% (Minarik & Watson, 1995). A power-law relationship between permeability $k(\phi)$ and melt concentration ϕ has been proposed by McKenzie (1984):

$$k(\phi) \propto a^2\phi^n \qquad (4)$$

where n is a dimensionless constant and a designates the characteristic diameter of the solid grains. When the melt flow is confined in tubes whose sizes increase with melt concentration, the power-law constant n is $\sim$2; in the case of a flow confined in intergranular films, $n \sim 3$ (McKenzie, 1984). Laboratory experiments with olivine and a basaltic melt suggest that the evolution of the shape of tubules with increasing melt concentration is complex and does not lead to a simple increase of their size (Faul, 1997). The same experiments show that melt flow is rapidly confined in disc-shaped intergranular films. As a result it is likely that in a kimberlite mush the permeability $k(\phi)$ follows a cubic relationship with melt concentration ϕ, i.e. $n \sim 3$ in equation (4).

Mantle rheology beneath cratonic lithosphere

It is generally accepted that the mantle in the 'asthenosphere' deforms by dislocation creep (Karato & Wu, 1993). As a result, the rate of deformation of the mantle rises as a power of the deviatoric stress. In the governing equations, the excess pressure p represents the deviatoric stress generated by viscous deformation. Thus, the plastic viscosity in a model representing melt percolation in the asthenosphere is excess pressure dependent. At the scale of the melt–solid grain interface the excess pressure corresponds to the deviatoric stress imposed along two adjacent faces of the grains (Sleep, 1988). As a result, the non-linear relationship between η and p probably reduces the amplitude of the excess pressure p [see equation (2) and discussion below] and, therefore, prevents the development of dykes by magma-fracturing. This explains Sleep's (1988) arguments to question the possibility of development of dykes by magma-fracturing in a partially molten mantle mush. Does this mean that magma-fracturing is impossible in a viscous mantle? We see that the problem crucially depends on the nature of the rheology of the mantle rock. Karato & Wu (1993) suggested that a relatively cold upper mantle at depths exceeding 100 km to 200 km deforms by along-grain diffusion creep. They based their arguments on the facts that: (1) the activation volume for dislocation creep is high and thus only favours deformation at low pressures; (2) the increase in the amplitude of the deviatoric stresses, from about 1 MPa to 10 MPa, in response to the decrease in rock ductility, because of the attenuation of the dislocation creep, leads to a reduction in the grain size of the mantle, which in turn enhances viscous flow by diffusion. Geophysical data supporting their model include the strong reduction in seismic anisotropy in the mantle at depth, and a cross-check between isostatic rebound data and modelling of the vertical movements triggered by deglaciation. In this study, we assume that the Karato & Wu (1993) hypothesis applies within the whole of the upper, viscously deforming mantle below the 100–200 km thick cratonic roots. As a result we assume that the viscosity of the mantle rock η is constant even when the excess pressure p is high. This hypothesis will be critically discussed in a subsequent section.

Nature of the obstruction triggering kimberlite melt concentrations

Ringwood *et al.* (1992), Nowell *et al.* (1999) and Sweeney & Winter (1999) proposed that Group 1 and Group 2 kimberlite magmas have a common parentage from a carbonate-bearing peridotite mantle source located at depths >300 km and containing various amounts of ancient subducted oceanic crust. The differences between the two kimberlite types are controlled by subsequent assimilation of variably enriched subcontinental lithospheric mantle (Nowell *et al.*, 1999; Sweeney & Winter, 1999). The kimberlite source rock is transported by mantle convection. When it ascends into the Transition Zone, i.e. within the 670–400 km depth interval, it melts to very low degree ($\phi < 1\%$) (e.g. Le Roex, 1986; Ringwood *et al.*, 1992; Haggerty, 1994; Nowell *et al.*, 1999). Kimberlitic melts wet the grain boundaries, creating an interconnected network with a non-zero permeability [$k(\phi)$, equation (4)]. Subsequently, the mantle mush comprising a low volume of kimberlite melt moves upward with the ascending mantle flow. Because of the newly created permeability, compaction develops within the partially molten mantle domain. During its intergranular upward percolation, the melt reacts with the minerals of the surrounding mantle rock (especially with garnet and orthopyroxene) to form clinopyroxene and other metasomatic minerals, inducing the progressive assimilation of the melt. After a few tens of kilometres of upward percolation, the melt is progressively assimilated. The kimberlite melt produced below pushes upward and is slowed down by the upward obstruction resulting from melt assimilation. This leads to a local accumulation of melt as a result of the reduction of the permeability in the downstream direction. The dramatic non-linear amplification of the permeability in the zone of melt accumulation enhances the melt concentration.

MODELLING THE DEVELOPMENT OF COMPACTION WAVES IN A SUB-CRATONIC KIMBERLITE MANTLE MUSH

Scales and dimensionless formulation of the equations

For the present treatment, it is necessary first to make the equations dimensionless. To achieve this, we adopt the following scales for measuring melt concentration ϕ_{sc} (where sc indicates scaled), pressure p_{sc}, length L, and time t_{sc}. The unit of length is the compaction length L (Rabinowicz *et al.*, 2002):

$$L = \frac{\sqrt{\eta k(\phi_{sc})}}{\mu \phi_{sc}}. \quad (5)$$

The excess pressure p_{sc} is given by

$$p_{sc} = \delta\rho g L. \quad (6)$$

This represents the pressure contrast between the solid and the magma integrated along the compaction length L.

The time t_{sc} is given by

$$t_{sc} = \eta / p_{sc}. \quad (7)$$

t_{sc} is the time taken for the melt in a mush with a constant concentration ϕ_{sc} to move upward over a distance of one compaction length, L. The values of L and t_{sc} depend on the parameters $\delta\rho$, ϕ_{sc}, $k(\phi_{sc})$, μ, and η, whose ranges need to be constrained. The value for the melt concentration ϕ_{sc} is equal to the degree of melting needed to produce kimberlite melt in the mantle, here assumed to be 0·6%, i.e. within the range proposed by Canil & Scarfe (1990) and Dalton & Presnall (1998). As suggested earlier, the density contrast between kimberlitic melt and the mantle, $\delta\rho$, is about 1000 kg/m^3 (Spera, 1984; McKenzie, 1985; Scarfe *et al.*, 1987). Maaløe & Scheie (1982) proposed a permeability $k(\phi_{sc})$ of $\sim 10^{-15}$ for rocks with millimetre-size grains [$a \sim 1$ mm, equation (4)] and melt fraction $\phi \sim 0{\cdot}01$. In the light of his experimental results, Faul (1997) suggested an order of magnitude lower permeability for a mush with the same characteristics. Typical grain sizes of mantle peridotites are ~3–4 mm. These sizes are typical of mantle rocks that deform by dislocation creep in the upper part of a relatively hot upper mantle. It has been nevertheless suggested by Karato & Wu (1993) that in a cold section of the upper mantle, below 150–200 km depth, the grain sizes will be small ($a \sim 1$ mm) to permit deformation of the rock by diffusion. As a consequence, because of the grain size and permeability models, we derived a $k(\phi_{sc} = 0{\cdot}6\%)$ of about 2×10^{-17} m^2 [see equation (4)]. The viscosities of kimberlite melts are known to be particularly low because of their low Si content and high concentrations of CO_2 and H_2O. However, the range of possible variation is large, from 0·01 to 1 Pa s, with a more probable value around 0·1 Pa s (McBirney & Murase, 1984; McKenzie, 1985, 1989). Following the study of Karato & Wu (1993), we strongly suspect that the plastic viscosity in the lower part of the upper mantle is constant and relatively high: various lines of evidence, particularly post-glacial rebound data, suggest a value of 10^{21} Pa s (Sabadini & Peltier, 1981; McBirney & Murase, 1984; McKenzie, 1989; Karato & Wu, 1993). Using equation (4) and the above parameters we, therefore, deduce that L ranges between 2 km and 18 km. We adopt here a value for L of 6 km, which is consistent with a kimberlite melt viscosity $\mu = 0{\cdot}1$ Pa s. We, therefore, deduce that the excess pressure is $p_{sc} =$ 60 MPa and the compaction time is $t_{sc} = 0{\cdot}5$ Myr [see equations (6) and (7), respectively].

The dimensionless versions of equations (2) and (3) are

$$\frac{\partial \phi'}{\partial t'} = \phi' p' \tag{8}$$

$$\nabla(\phi'^n \nabla p') - \phi' p' = \frac{\partial(\phi'^n)}{\partial z'} \tag{9}$$

where $\phi' = \phi/\phi_{sc}$, $p' = p/p_{sc}$, $t' = t/t_{sc}$ and $z' = z/L$ designate the dimensionless variables. It should be noted that this system of equations does not depend on any dimensionless parameter. In fact, the only 'free parameter' is the dimensionless melt concentration profile used to initiate the computations. As shown below [equation (10)], this function depicts how melt is produced and thereafter assimilated by reaction with the surrounding minerals.

Evolution of the melt concentration during a compaction experiment

The experiment shown in Fig. 3 was run in a computing box of 450 km × 450 km size, i.e. with a dimensionless size of 75 × 75. To save grid points, the flow is periodic along z with a periodicity of 450 km, i.e. a dimensionless periodicity of 75, and is symmetrical on both lateral faces of the computing box. The melt concentration equation [equation (8)] is solved with a second order in time and in space explicit finite difference scheme (Barcilon & Richter, 1986). The pressure equation [equation (9)] is discretized with the fourth-order-in-space scheme proposed by Barcilon & Richter (1986). The equation is solved with a multi-grid method. The numerical method is that used by Wiggins & Spiegelman (1995) to resolve 3-D compaction problems. Our code has been benchmarked in previous studies (Rabinowicz & Ceuleneer, 2005). We used 256 × 256 equidistant grid points along the horizontal axis, x, and the vertical axis, z.

The experiment was initiated with the following dimensionless melt distribution function:

$$\phi_n(x', z') = \phi_{sc} \frac{[1 + ra(x')]}{\cosh(0{\cdot}3 \times z'_d)} \tag{10}$$

where $ra(x')$ is a random function with a mean amplitude of 0·05, $z'_d = \min(z', 75\,\text{km} - z')$. It implies that, in this experiment, melt assimilation occurs between a dimensionless height z' of 0–10, i.e. a dimensional height of 0–60 km, which represents the several tens of kilometres estimated thickness of the kimberlite melt assimilation zone (see above). Because of the vertical periodicity, the production of melt in the model occurs at a dimensionless depth of about 0–10 below the bottom of the computing box.

The evolution of the melt concentration and the excess pressure during a time period of 27 × t_{sc} ~13·5 Myr is shown in Fig. 3. First the kimberlite melt accumulates at the top of the obstruction zone. The thickness of this first zone of high melt concentration depends on the characteristic length of the solid deformation term $\nabla(\phi'^n \nabla p')$, which represents several times the compaction length L (Ribe, 1985). Because of mass conservation [equation (8)] the mush permeability, the melt concentration and the velocity sharply decrease below the zone concentrated in melt, which is therefore hydraulically disconnected from the bulk of the mush. This process triggers the splitting of the mush into compaction waves (see Rabinowicz *et al.*, 2002). Then the porosity waves develop in three stages: (1) equidistant planar waves are triggered just below the top of the field of high melt concentration; (2) at about a time of 13·5 × t_{sc} ~7 Myr, spherical melt pockets are generated inside the planar waves and collect melt up to a concentration of 7%, i.e. a dimensionless concentration ϕ' of ~12; (3) the melt pockets are separated from the horizontal waves and follow their own trajectories, leading them to collide with some of those found along their path. The characteristic dimensionless size of the pockets is approximately six: i.e. their dimensional size is $6 \times L \sim 36$ km. In fact, this size depends on the sharpness of the assimilation front in the initial melt concentration profile. In the experiment shown in Fig. 3 the drop in melt concentration occurs over a dimensionless distance of ~10 (Fig. 3). Other experiments show that when this drop occurs over a smaller length, the wave size decreases to two and the growth rate and asymptotic amplitude of the waves increase. This type of experiment has already been the purpose of several 2-D or 3-D numerical studies (Wiggins & Spiegelman, 1995; Rabinowicz & Ceuleneer, 2005).

Transient development of the excess pressure during the compaction experiment

To gain an insight into melt redistribution during compaction, we have studied more precisely the transient evolution of the excess pressure p inside a compaction wave. Figure 4 shows a vertical profile of both p' and ϕ' taken at the end of the experiment along the left lateral boundary of the computing box. At the top and bottom of each individual wavelet, the excess pressure field p' reaches its maximum and minimum, respectively. Therefore, at the top of a wavelet the pressure of the fluid is greater than that of the rock. Accordingly, the mush is dilated and the melt is propelled upward. At the same time, at the bottom of a wavelet, the pressure of the solid exceeds that of the melt, and the rock squeezes the melt column that escapes upwards. The wavelets being symmetrical, the amplitude of the pressure maxima is the same as that of the minima. It should be noted that in a wavelet the pressure linearly increases from its minimum up to its maximum, and it dramatically shrinks just above

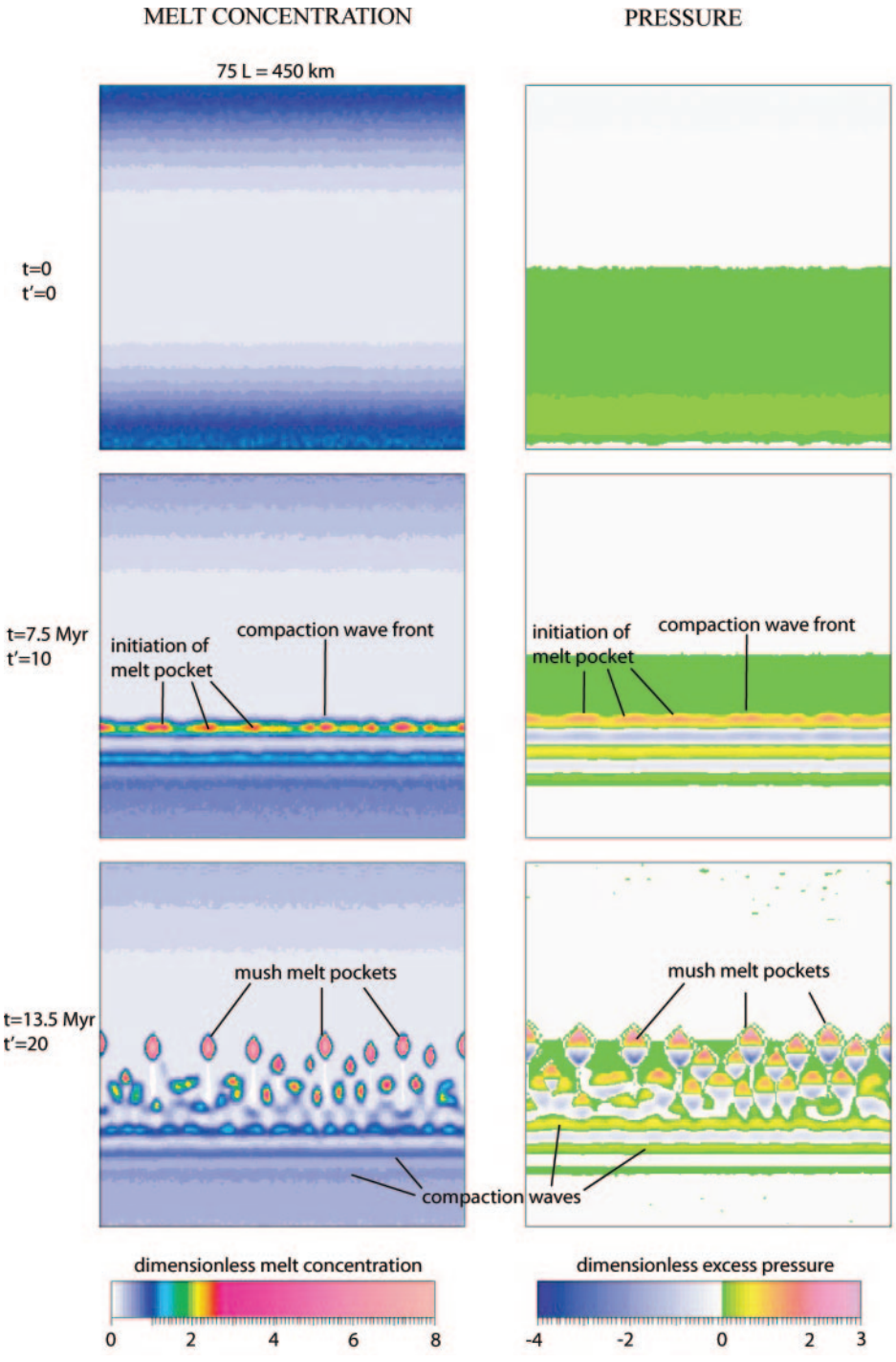

Fig. 3. Compaction experiment. From top to bottom are drawn the $t' = 0$, $t' = 13{\cdot}5$ ($t = 7{\cdot}5$ Myr), and time $t' = 27$ ($t = 13{\cdot}5$ Myr) snapshots of the dimensionless melt concentration and excess pressure fields in an experiment with a computing box size of $75L$ (450 km). The experiment was initiated with a melt distribution function given by equation (10). The values of the parameters are given in Table 2. At time 13·5 (≈7·5 Myr), the wave front is planar, but inside the top wave several pockets are initiated. Thereafter, the planar wave splits and each pocket is individualized. At the end of the experiment, occurring at time 27 (≈13·5 Myr), the first swarm of melt pockets has moved up by about $25L$ (≈150 km), i.e. with a mean upward velocity of about 1 cm/year. They have a width of about $6L$ (≈36 km), and the maximum melt concentration reached inside the pockets is about $12\phi_{sc}$, i.e. about 7%. It should be noted that there is a strong interaction between melt pockets generated inside successive planar waves. At the top of each pocket, excess pressure reaches a maximum of about $3{\cdot}2 \times p_{sc} = 200$ MPa, a value high enough to trigger the fracture of the overlying rock (>40–50 MPa).

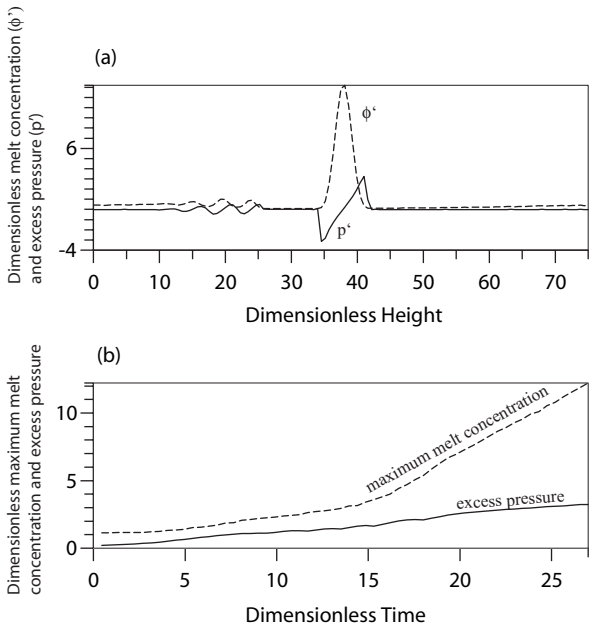

Fig. 4. (a) The dimensionless melt concentration ϕ' (dashed line), and the excess pressure p' vertical profile (continuous line) taken at time 27 along the left lateral face of the model of Fig. 3. (b) The time evolution of the maximum melt concentration (dashed line) and the excess pressure (continuous line) during the numerical experiment. It should be noted that the maximum pressure and melt concentration increase linearly and quadratically with time, respectively. The excess porosity scale factor $\phi_{sc} = 0{\cdot}6\%$, and the pressure scale factor $p_{sc} = 60$ MPa. The excess pressure [equation (6)] results from the density contrast between the melt and the solid fraction of the mush ($\delta\rho$). It is thus proportional to $\delta\rho gL$. More precisely, an excess pressure of about $3 \times \delta\rho gL$ is expected at the top of the pocket, a value high enough to trigger fracturing.

the top of the wavelet and just below its bottom, respectively. During the transient development of the compaction wave, both the amplitude of the melt concentration ϕ' and the pressure p' markedly increase with time. Figure 4b shows the maximum excess pressure p' and melt concentration ϕ' of the wave train as a function of dimensionless time. We see that the maximum excess pressure linearly increases with time whereas the maximum melt concentration in the wave follows a quadratic path. When the experiment is initiated, the amplitude of the excess pressure p' is negligible. At the end of the experiment, i.e. at dimensionless time 27, the excess pressure is about 3·2.

These striking results can be explained as follows. When the experiment is initiated, the gradient of pressure in the melt column roughly balances the difference in weight between melt and solid [see equations (3) and (9)]. Accordingly, the pressure in the fluid is close to that in the solid, and the excess pressure p' is extremely small. As the amplitude of the compaction wave increases, melt circulation within the wavelet increases because the permeability of the mush becomes extremely large in the regions of high melt concentration [see equation (4)]. As a result, the pressure drop inside the melt column is small, promoting a large increase in the pressure difference between the melt and the solid, and thus of the excess pressure field in the wave. This explains why, at the end of the experiment, the difference in excess pressure between the bottom and the top of the wavelet is about $2 \times 3{\cdot}2 = 6{\cdot}4$. The latter value roughly represents the difference between the lithostatic and the hydrostatic pressure across a wavelet with a dimensionless size of about six.

Now if we consider dimensional variables, we see that the excess pressure p at the top of the compaction pockets reaches a value of $3{\cdot}2\ p_{sc} \sim 200$ MPa. This value exceeds by a factor of four the estimated fracture threshold of the rock. It also exceeds by a factor of 20 the deviatoric stress generated by mantle convection in the lower part of the upper mantle (about 10 MPa; Rabinowicz *et al.*, 1980). These numbers show that the hypothesis that the deformation of the mantle beneath the cratonic lithosphere is governed by diffusion creep is fundamental for the coherence of our model because in the case of mantle deforming by dislocation creep, the rise of the excess pressure p above a level of 100 MPa would cause a drop of the effective viscosity η_{eff} at the top of the compaction wave by at least three orders of magnitude. Consequently, the 'effective compaction length' L_{eff}, which rises as $\sqrt{\eta_{eff}}$ [see equation (5)], and the dimensional excess pressure p_{eff}, which is proportional to L_{eff} [see equation (6)], are expected to drop by a factor of 30. As a result, the excess pressure would fall below the 50 MPa fracture threshold. These results corroborate those developed by Sleep (1988). We see thus that only a diffusion creep rheology in the sub-cratonic mantle permits the development of fracturing at the top of the compaction waves. The experiment shows that mature compaction pockets need a period of time of about $20t_{sc} \sim 10$ Myr to be generated. During this time period, the compaction front moves upwards by <150 km. The model assumes a reference frame pegged to the convective mantle. As a result, the true upward migration of the melt is the sum of the height of melt percolation plus the height of upward migration of the mantle in the ascending flow during the period of maturation of the melt compaction pocket. If we assume 1 or 2 cm/year upward movement as a result of mantle convection, the melt would rise by 250–350 km before the maturation of a compaction pocket would be achieved. This height is similar to that estimated for the ductile part of the upper mantle beneath a craton. Otherwise, if the convective current is fast, for example, 10 cm/year, a possible value in the centre of a hot cylindrical mantle plume, the compaction front would collide with the base of the cratonic lithosphere well before the excess pressure of a compaction pocket

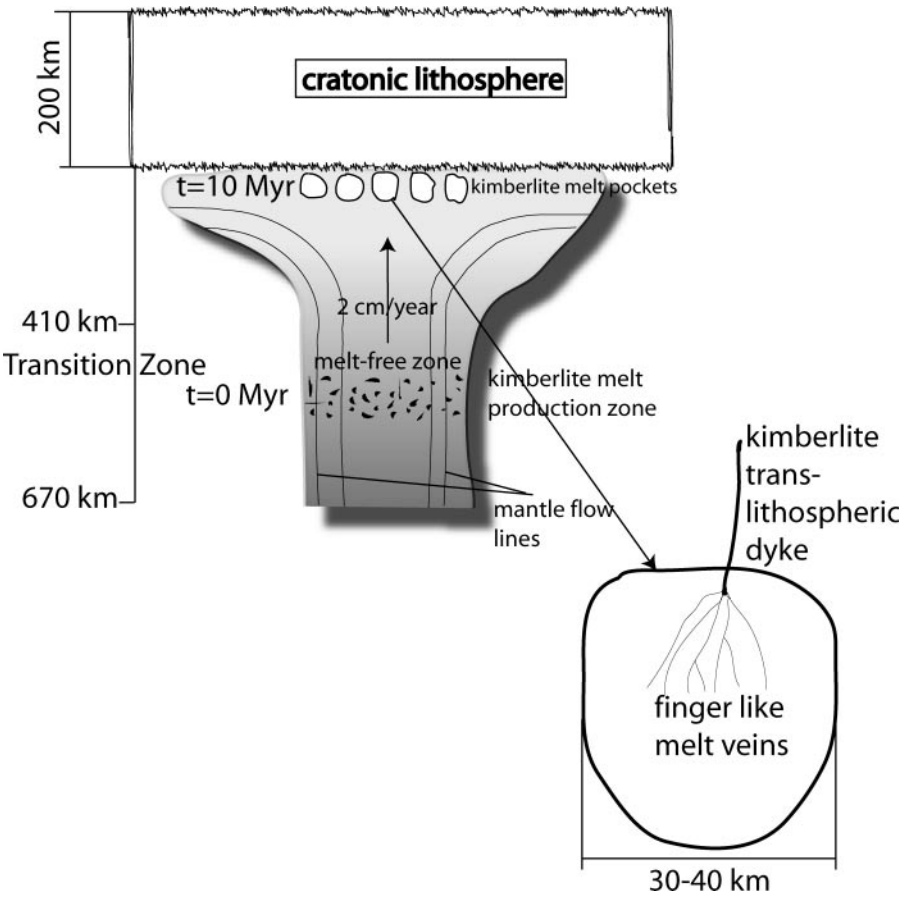

Fig. 5. Sketch map of the proposed model in a context of subcratonic upper mantle flow. We consider, below a cratonic lithosphere about 200 km thick, a mantle domain 450 km in size ascending upward at a velocity of 2 cm/year. At time $t = 0$, a kimberlite melt-bearing horizon, about 60 km thick, is produced within the Transition Zone and moves upwards with the mantle flow. After 10 Myr this horizon has ascended by 200 km and at the same time the top of the compaction wave has percolated through the permeable mantle matrix by about 120 km. Kimberlite melt-bearing pockets of about 30–40 km in diameter have been generated in this wave. In the mush melt pocket two zones are favourable for the development of 'dykes'. The first, corresponding to the zone of initiation of the translithospheric kimberlites reaching the surface of the Earth and entraining mantle xenoliths, is localized at the top of the pocket, where the excess pressure is positive and high, and the melt concentration extremely low. The second zone, corresponding to the zone of generation of thin veins as described by Rubin (1998), is localized in the middle of the pocket, where melt concentration is extremely high and the excess pressure is small.

would be capable of breaking the melt-free rock in the roof of the pocket.

DYKE GENERATION IN MUSH MELT POCKETS

In Figure 5 we place our model in the context of subcratonic upper mantle flow. We consider a mantle domain 450 km in width ascending upward at a velocity of a few centimetres a year (assumed to be 2 cm/year in Fig. 5). At time $t = 0$, a kimberlite melt-bearing horizon, about 60 km thick, is produced within the Transition Zone (Fig. 5), which moves upwards with the mantle flow. After 10 Myr this horizon has ascended by 200 km and at the same time the top of the compaction wave has percolated through the permeable mantle matrix by about 120 km. Kimberlite melt-bearing pockets of about 30–40 km diameter have been generated in this wave. In these mush melt pockets two zones are favourable for the development of 'dykes' (Fig. 5). The first is localized at the top of pockets, where the excess pressure is positive and high, and the melt concentration extremely low; the second is localized in the middle of the pocket, where melt concentration is extremely high and the excess pressure is small. The causes of dyking differ in the two regions.

Dyke generation from the top of the mush melt pockets

Here, the excess pressure probably reaches $p_{sc} = \delta\rho gL$, i.e. 60 MPa. This exceeds the tensile strength of the melt-free mantle, $\sigma_c \sim 40$ MPa (Spera, 1987; Rubin, 1995).

Considering that the melt fraction at the top of the melt pocket is only a fraction of the value $\phi_{sc} = 0{\cdot}6\%$ used in our model (see above), i.e. a few times 0·1%, the failure criterion is clearly that of the melt-free rock. Accordingly, fracturing of the mantle wall-rock is unavoidable, and the condition for the generation of a magma crack is realized. In the crack, the excess pressure drops, triggering a transient flowing melt, which accumulates in the crack (Sleep, 1988). When the differential pressure as a result of the difference of density between the magma in the crack and the solid rock column exceeds the tensile strength σ_c, the crack propagates upward, fracturing the melt-free cap rock. The failure criterion is reached when the height of the crack is l–4 km. According to equation (1), the width of the crack is $\Delta l = \sigma_c l/M$; for $M \sim 50$ GPa (Rubin, 1995), we find that the crack width Δl is about 2–3 m, in agreement with the maximum width of kimberlitic dykes observed at the surface.

Dyke generation from the middle of the mush melt pockets

In the middle of the melt mush pocket, the excess pressure is probably too small to promote the fracturing of melt-free mantle rock. Because of the high melt concentration, the interstitial melt films wet a significant fraction, if not all, of the grain surfaces. Accordingly, the tensile stress needed to fracture the mush is probably small: $\sigma_c \sim 1$ MPa. Rubin (1998) suggested that the deviatoric stresses generated by mantle convection, with an amplitude of a few megapascals, could lead to the nucleation of numerous small melt-filled cracks in the mush. In the crack, the local pressure drop resulting from the crack opening drives a Darcy flow of melt inside the crack. Rubin (1998) showed that the coupling of the local Darcy flow and the upper tip propagation leads to the development of finger-like dykes several kilometres long, oriented parallel to the direction of maximum compression σ_1. A robust result of Rubin's (1998) model is that such finger-like dykes are only a few millimetres thick. We propose that when a horsetail-like set of finger-like dykes meets the top of the mush pocket, they merge to form a melt-filled crack several kilometres high and several metres wide, which propagates upward through the upper mantle by fracturing the melt-free cap rock.

DISCUSSION

Our model is based on the observation that: (1) kimberlites occur only in areas characterized by a thick lithosphere (150–200 km) originating in a plastic zone of the mantle that deforms by diffusion creep, and the assumptions that (2) kimberlitic melts result from low degrees of partial melting at great depth of carbonated peridotites in slowly ascending mantle flows, (3) these melts are, thereafter, partly assimilated by reaction with surrounding mantle minerals and (4) at these depths the mantle is viscous enough for the compaction length to reach a value of about 6 km. If these conditions are met, compaction processes may cause large increases in the local concentration of kimberlite melt (up to 7%) and form melt-bearing pockets a few tens of kilometres across. In this case, the dynamic imbalance between hydrostatic and lithostatic pressure drives the upward migration of the localized melt body. At the top of the wave the positive excess pressure dilates the mush, whereas at the bottom it compacts it. Our model shows that in a matured pocket, the maximum amplitude of the excess pressure and the depression at the top and bottom of the structure is about equal to half the amplitude of the pressure difference between the solid and melt, integrated along the vertical section of the body. In this case, the initiation of swarms of dykes is inevitable because of the large excess of pressure at the top of the mush melt pockets, $3 \times p_{sc} \geq 150$ MPa, which is much higher than the hydraulic fracturing limit of the overlying rocks (30–50 MPa; Spera, 1987; Rubin, 1993).

Our model provides an explanation for the origin of the deformed high-T garnet peridotite xenoliths entrained by kimberlites and equilibrated at pressures ranging from 4·5 to >6·5 GPa (i.e at depths ranging from 150 to 250 km). The significance of their textures has been of considerable interest since their original recognition by Nixon & Boyd (1973). Proposals for their generation include shear zones, shear heating or deformation during diapiric upwelling (e.g. Downes, 1990; Van Thienen *et al.*, 2003). They strongly suggest that the xenoliths were plastic when they were sampled by the kimberlite magmas. Accordingly, they do not belong to the lithospheric mantle but to the underlying 'asthenosphere'. Whatever the cause, porphyroclastic textures cannot be retained for long periods in the deep part of the mantle (e.g. Goetze, 1975; Pearson *et al.*, 2003). Porphyroclastic textures are thus transient phenomena experienced by samples on a short time scale before entrainment in their host magma, as is also indicated by the zoning patterns in minerals from these rocks (Smith & Boyd, 1992; Pearson *et al.*, 2003). We propose that the porphyroclastic and mosaic-porphyroclastic textures of the deformed high-T and high-P garnet peridotite xenoliths entrained by kimberlites result from plastic deformation at the top of the melt pockets caused by the large excess of pressure. This deformation of the roof of the melt pockets happened shortly before entrainment of xenoliths in the host kimberlite.

In our model the estimated size of the melt-bearing pockets is similar to the average dimensions of kimberlite fields (30–50 km, Figs 1 and 2). We, therefore, propose that kimberlite fields are the surface envelope of dyke swarms generated inside a mush melt pocket and that

a kimberlite cluster represents the discharge of melt via dykes originating from a sub-region of a mush pocket. According to our model, these dykes should have lensoidal shapes with a typical diameter of 4 km and a maximum thickness of 3 m. We propose that these lens-shaped dykes cross-cut the lithosphere.

During intrusion the dykes sample the surrounding upper mantle rocks as xenoliths with a size range up to 1 m (typically 5–20 cm). The two main mechanisms of xenolith formation in the lithosphere are: (1) fracturing of wall-rock during kimberlite dyke propagation; (2) progressive detachment of fragments as a consequence of magma intrusion along fractures parallel to the dykes (e.g. Morin & Corriveau, 1996). The surrounding peridotite wall-rocks clearly need to be fractured for kimberlite dykes to initiate and propagate. Their resistance to fracturing is easily exceeded by the magma pressure (Spera, 1984; Pollard, 1987; this study). Model calculation and experiments indicate that inelastic deformation occurs at the leading edge of a propagating dyke (e.g. Maaløe, 1987; Rubin, 1993). At high confining pressures, this deformation may result in a set of dyke-parallel fractures extending to tens of metres from the dyke contact (Pollard, 1987; Rubin, 1993). Once the fracture set is created magma eventually invades the fractures to form apophyses; country-rock fragments are progressively detached and the rapidly ascending magma filling the dyke entrains the xenoliths upward (e.g. Morin & Corriveau, 1996, fig. 6). Many of these mantle xenoliths display evidence of metasomatic reactions with kimberlite magma at depth, and the local development of some millimetre-wide dykelets (Erlank *et al.*, 1987; Grégoire *et al.*, 2002, 2003). These dykelets may correspond to the finger-like dykelets proposed by Rubin (1998). The time required in our model to reach the excess pressure in a melt pocket is several million years. At greater time scales the maximum excess pressure in the pocket will be constrained by the hydraulic fracture limit of the rock cap. That implies that the melt concentration within the pocket will be stabilized and the melt coming from below will be periodically evacuated by dykes. At the same time, at the top of the pocket, part of the melt will be incorporated as an intergranular film within the surrounding peridotite.

The compaction problem depends on two independent parameters: (1) a geometrical parameter, i.e. the compaction length L [equation (5)]; (2) a time parameter, the time scale $t_{sc} = \eta/p_{sc}$ (equation (7)]. Hydraulic fracture requires that $3 \times p_{sc}$ ($= \delta\rho gL$) exceeds 400–500 MPa at the top of the melt pocket. Given that gL is $\sim$1000 kg/m^3, we can predict that L will exceed 1 km, producing melt pockets with a minimum diameter of 6 km. Given the small range in the reported characteristic size of kimberlite fields range (30–50 km) (Janse, 1984; Garanin *et al.*, 1993; Basson & Viola, 2003), we infer that the uncertainty in compaction length is small, typically $L = 6 \pm 1$ km. The determination of L also has a major effect on the time needed to generate mush melt pockets. For example, assuming a value for L of only 1 km would lead to a time of melt pocket generation of about 60 Myr, a value considerably lower than the time it takes for an ascending flow moving at 1 cm/year to cross the whole plastic section of the upper mantle (40 Myr; McKenzie, 1984). The other parameter controlling the time of pocket generation is the solid viscosity of the mantle. The value of 10^{21} Pa s used here (Table 2) is a typical estimate for the mantle Transition Zone below cratonic regions (Karato & Wu, 1993). A significantly higher value will lead to a maturation time of the melt pocket also greatly exceeding the time taken for the upwelling to cross the upper mantle. On the other hand, it is possible that the viscosity inside a hot flow could be an order of magnitude lower than 10^{21} Pa s (Monnereau *et al.*, 1993). For instance, Sleep (2003) suggested a value of $\sim 10^{19}$ Pa s. Assuming this latter value, and maintaining a compaction length L of about 6 km, we predict a time scale of generation of melt pockets of the order of 10^5 years, i.e. quasi-instantaneous. If the production of kimberlite melts starts well within the Transition Zone, as suggested by some studies (Ringwood *et al.*, 1992; Haggerty, 1994), a value of 10^{19} Pa s for mantle viscosity implies a zone of initiation of the kimberlite dykes at 120 km above the source region, i.e. at a depth below 300 km (Fig. 5). The deepest mantle xenoliths entrained by kimberlites come from about 200 km, inconsistent with this predicted depth of dyke initiation. This conclusion does not exclude mantle viscosity of 10^{19} Pa s, but in this case the production zone of kimberlite melt must occur above 300 km, a value not incompatible with other estimations of the depth of kimberlite source regions (Canil & Scarfe, 1990; Dalton & Presnall, 1998). A further point of interest is that the range of the ages of kimberlite dykes and pipes in a given field should provide strong constraints on mantle dynamics below cratons. If we trust the age range of 10 Myr deduced from precise and numerous isotopic studies of the Kimberley

Table 2: Values of the main parameters used in and estimated from the model

ϕ_{sc}	0·6%
$\delta\rho$	1000 kg/m^3
$k(\phi_{sc} = 0{\cdot}6\%)$	2×10^{-17} m^2
a	1 mm
μ	0·1 Pa s
η	10^{21} Pa s
L	6 km
p_{sc}	60 MPa

Kimberlite field (Kaapvaal craton, South Africa) we are forced to conclude that the mantle has a solid viscosity of 10^{21} Pa s and that production of kimberlite melt occurs within the lower part of the Transition Zone. Conversely, if future precise isotopic dating of kimberlite dykes and pipes in a specific field gives a range of about 1 Myr, this would provide strong evidence in favour of lower solid viscosity of the plastic mantle transporting the kimberlite melts and a shallower melt source region. This last hypothesis is in good agreement with the model proposed by Sleep (2003) for the generation of kimberlite fields.

It is also interesting to note that the typical kimberlite districts define domains of a few hundred kilometres, i.e. of the same order of magnitude as that of a typical mantle convective flow in the mantle Transition Zone (Davaille, 1999; Montelli *et al.*, 2004). It is likely that such flows horizontally migrate with a velocity <1 cm/year. Accordingly, it appears probable that in a district all the kimberlite fields that have been formed over $\sim$20 Myr are the surface expressions of the same phase of activity of an ascending convective flow. If we apply this hypothesis to the case of the Kimberley district (Fig. 2), at least four fields comprising pipes and dykes of Group 1 kimberlites (Kimberley, part of Barkly West, Rietfontein and Koffiefontein) may have been generated this way at 80–90 Ma, and at least three others (part of Barkly West, Newlands and Finsch) at 115–120 Ma. At the scale of the Kaapvaal craton, we propose that the main part of the districts of Kimberley, N. Lesotho and Orapa, constituted by Group 1 kimberlites and dated at 80–90 Ma (Fig. 2), have been formed from the same ascending mantle flow (Davaille, 1999; Montelli *et al.*, 2004). The same model could apply to the Group 1 kimberlites of the Rietfontein, Central Cape and Gibeon districts but at 60–70 Ma (Fig. 2). Finally, we could speculate that the flow that produced the three districts at 80–90 Ma migrated westward by few hundred kilometres to form the three districts dated at 60–70 Ma.

Once generated, the dyke swarms propagate along a direction parallel to the maximum compressive stress, which in an ascending convective flow, gives them near-vertical orientation (Rabinowicz *et al.*, 1984). Because of its great thickness, the cratonic lithosphere is generally under compression (Zoback & Mooney, 2003). Hence, the dyke trajectories could become horizontal when they penetrate the lithosphere. The extensional stresses generated by a convective flow at its top overcome the compressive stresses that normally act in the cratonic lithosphere, but probably only at depth. An extensional tectonic regime affecting the entire cratonic lithosphere is required to allow the arrival of the dyke swarms at the surface. This is consistent with the findings of recent studies concluding that structural control of the emplacement of kimberlites on the Kaapvaal craton is related to extensional tectonics (White *et al.*, 1995; Basson & Viola, 2003). If the compressive lithospheric stress remains locally very high, the kimberlite dykes will be emplaced as sills and the kimberlites will not reach the surface.

ACKNOWLEDGEMENTS

This research was supported by INSU-DyETI Program. We thank W. L. Griffin, G. Ceuleneer and A. Rubin for their constructive comments on an early version of the manuscript. Constructive reviews by N. Sleep, S. Maaløe and F. Spera greatly improved the manuscript. Special thanks go to the chief editor M. Wilson, who did a very careful additional review of the manuscript.

REFERENCES

Allsopp, H. L. & Barrett, D. R. (1975). Rb–Sr age determinations on South African kimberlite pipes. *Physic and Chemistry of the Earth* **9**, 619.

Allsopp, H. L., Bristow, J. W., Smith, C. B., Brown, R., Gleadow, A. J. W., Kramers, J. D. & Garvie, O. G. (1989). A summary of radiometric dating methods applicable to kimberlites and related rocks. In: Ross. J. (ed.) *Proceedings of the 4th International Kimberlite Conference, 1*. Perth: Geological Society of Australia, pp. 343–357.

Barcilon, V. & Richter, F. M. (1986). Non-linear waves in compacting media. *Journal of Fluid Mechanics* **164**, 429–448.

Basson, I. J. & Viola, G. (2003). Structural overview of selected Group II kimberlite dyke arrays in South Africa. *South African Journal of Geology* **106**, 375–394.

Bercovici, D., Ricard, Y. & Schubert, G. (2001). A two phase model for compaction and damage, 1, general theory. *Journal of Geophysical Research* **106**, 8887–8906.

Canil, D. & Scarfe, C. M. (1990). Phase relations in peridotite + CO_2 systems to 12 GPa: implication for the origin of kimberlite and carbonate stability in the Earth's mantle. *Journal of Geophysical Research* **95**, 15805–15816.

Chalot-Prat, F. & Boullier, A. M. (1997). Metasomatism in the subcontinental mantle beneath the Eastern Carpathians (Romania): new evidence from trace element geochemistry. *Contributions to Mineralogy and Petrology* **129**, 284–307.

Dalton, J. A. & Presnall, D. C. (1998). The continuum of primary carbonatitic–kimberlitic melt compositions in equilibrium with lherzolite: data from the system CaO–MgO–Al_2O_3–SiO_2–CO_2 at 6 GPa. *Journal of Petrology* **39**, 1953–1964.

Dautria, J. M., Dupuy, C., Takherist, D. & Dostal, J. (1992). Carbonate metasomatism in the lithospheric mantle: peridotite xenoliths from a melilititic district of the Sahara basin. *Contributions to Mineralogy and Petrology* **111**, 37–52.

Davaille, A. (1999). Simultaneous generation of hotspots and superswells by convection in a heterogeneous planetary mantle. *Nature* **402**, 756.

Downes, H. (1990). Shear zones in the upper mantle—relation between chemical enrichment and deformation in mantle peridotites. *Geology* **18**, 374–377.

Erlank, A. J., Waters, F. G., Hawkesworth, C. J., Haggerty, S. E., Allsopp, H. L., Rickard, R. S. & Menzies, M. (1987). Evidence for mantle metasomatism in peridotite nodules from the Kimberley pipes, South Africa. In: Menzies, M. & Hawkesworth, C. J. (eds) *Mantle Metasomatism*. London: Academic Press, pp. 221–309.

Faul, U. H. (1997). Permeability of partially molten upper mantle rocks from experiments and percolation theory. *Journal of Geophysical Research* **102**, 10299–10311.

Fowler, A. C. (1984). On the transport of moisture in polythermal glaciers. *Geophysical and Astrophysical Fluid Dynamics* **28**, 99–140

Garanin, V. K., Kudryavtseva, G. P. & Janse, A. J. A. (1993). Vertical and horizontal zoning of kimberlites. In: Maurice, T. (ed.) *Proceedings of the 8th IAGOD Symposium*. Ottawa, Ont., pp. 435–443.

Goetze, C., (1975). Sheared lherzolites: from the point of view of rock mechanics. *Geology* **3**, 172–173.

Green, D. H. & Wallace, M. E. (1988). Mantle metasomatism by ephemeral carbonatite melts. *Nature* **336**, 459–462.

Green, H. W., II & Gueguen, Y. (1974). Origin of kimberlite by diapiric upwelling in the upper mantle. *Nature* **249**, 617–620.

Grégoire, M., Moine, B. N., O'Reilly, S. Y., Cottin, J. Y. & Giret, A. (2000). Trace element residence and partitioning in mantle xenoliths metasomatized by high alkaline silicate- and carbonate-rich melts (Kerguelen Islands, Indian Ocean). *Journal of Petrology* **41**, 477–509.

Grégoire, M., Bell, D. R. & Le Roex, A. P. (2002). Trace element geochemistry of glimmerite and MARID mantle xenoliths: their classification and relationship to phlogopite-bearing peridotites and to kimberlites revisited. *Contributions to Mineralogy and Petrology* **142**, 603–625.

Grégoire, M., Bell, D. R. & Le Roex, A. P. (2003). Garnet lherzolites from the Kaapvaal craton (South Africa): trace element evidence for a metasomatic history. *Journal of Petrology* **44**, 629–657.

Griffin, W. L., Gurney, J. J. & Ryan, C. G. (1992). Variations in trapping temperatures and trace elements in peridotite-suite inclusions from African diamonds: evidence for two inclusion suites, and implications for lithosphere stratigraphy. *Contributions to Mineralogy and Petrology* **110**, 1–15.

Gurney, J. J., Moore, R. O., Otter, M. L., Kirkley, M. B., Hops, J. J. & McCandless, T. E. (1991). Southern African kimberlites and their xenoliths. In: Kampunzu, A. B. & Lubala, R. T. (eds) *Magmatism in Extensional Structural Settings*. Berlin: Springer, pp. 496–535.

Haggerty, S. E. (1994). Superkimberlites: a geodynamic diamond window to the Earth's core. *Earth and Planetary Science Letters* **122**, 57–69.

Harris, J. W. (1992). Diamond geology. In: Field, J. E. (ed.) *The Properties of Natural and Synthetic Diamond*. London: Academic Press, pp. 345–393.

Helmstaedt, H. H. & Gurney, J. J. (1997). Geodynamic controls of kimberlites—what are the roles of hotspots and plate tectonics? In: Sobolev, N. V. & Mitchell, R. H. (eds) *6th International Kimberlite Conference Volume 2, Diamonds: Characterization, Genesis and Exploration*. New York: Allerton Press, pp. 394–404.

Hess, P. C. (1994). Thermodynamics of thin fluid films. *Journal of Geophysical Research* **99**, 7219–7229.

Hunter, R. H. & McKenzie, D. (1989). The equilibrium geometry of carbonate melts in rocks of mantle composition. *Earth and Planetary Science Letters* **92**, 347–356.

Ionov, D. A. (1998). Trace element composition of mantle-derived carbonates and coexisting phases in peridotite xenoliths from alkali basalts. *Journal of Petrology* **39**, 1931–1941.

Janse, A. J. A. (1984). Kimberlites, where and when? In: Glover, J. E. & Harris, P. G. (eds) *Kimberlite Occurrence and Origin: a Basis for Conceptual Models in Exploration. Department of Geology and University Extension, University of Western Australia, Publication* **8**, 19–62.

Karato, S. I. & Wu, P. (1993). Rheology of the upper mantle: a synthesis. *Science* **260**, 771–778.

Kramers, J. D., Roddick, J. C. M. & Dawson, J. B. (1983). Trace element and isotopic studies on veined, metasomatic and 'MARID' xenoliths from Bultfontein, South Africa. *Earth and Planetary Science Letters* **65**, 90–106.

Le Maitre, R. W. (2002). *A Classification of Igneous Rocks and Glossary of Terms*. Cambridge: Cambridge University Press, 236 pp.

Le Roex, A. P. (1986). Geochemical correlation between southern African kimberlites and South Atlantic hotspots. *Nature* **324**, 243–245.

Lorenz, V., Zimanowski, B., Büttner, R. & Kurszlaukis, R. S. (1999). Formation of kimberlite diatremes by explosive interaction of kimberlite magma with groundwater: field and experimental aspects. In: Gurney, J. J., Gurney, J. L., Pascoe, M. D. & Richardson, S. H. (eds) *The P. H. Nixon Volume. Proceedings of the 7th International Kimberlite Conference*. Cape Town: Red Roof Design, pp. 522–528.

Maaløe, S. (1987). The generation and shape of feeder dykes from mantle sources. *Contributions to Mineralogy and Petrology* **96**, 47–55.

Maaløe, S. (2003). Melt dynamics of a partially molten mantle with randomly oriented veins. *Journal of Petrology* **44**, 1193–1210.

Maaløe, S. & Scheie, S. M. (1982). The permeability controlled accumulation of primary magma. *Contributions to Mineralogy and Petrology* **81**, 350–357.

McBirney, A. & Murase, T. (1984). Rheological properties of magmas. *Annual Review of Earth and Planetary Sciences* **12**, 337–357.

McKenzie, D. (1984). The generation and compaction of partially molten rock. *Journal of Petrology* **25**, 713–765.

McKenzie, D. (1985). The extraction of magma from the crust and mantle. *Earth and Planetary Science Letters* **74**, 81–91.

McKenzie, D. (1989). Some remarks on the movement of small melt fractions in the mantle. *Earth and Planetary Science Letters* **95**, 53–72.

Minarik, W. G. & Watson, E. B. (1995). Interconnectivity of carbonate melt at low melt fraction. *Earth and Planetary Science Letters* **133**, 423–437.

Mitchell, R. H. (1995). *Petrology of Kimberlites, Orangeites and Related Rocks*. New York: Plenum, 410 pp.

Monnereau, M., Rabinowicz, M. & Arquis, E. (1993). Mechanical erosion and reheating of the lithosphere: a numerical model for hotspots swells. *Journal of Geophysical Research* **98**(B1), 809–823.

Montelli, R., Nolet, G., Dahlen, F. A., Masters, G., Engdahl, E. R. & Hung, S. H. (2004). Finite-frequency tomography reveals a variety of plumes in the mantle. *Science* **303**, 338–343.

Morin, D. & Corriveau, L. (1996). Fragmentation processes and xenolith transport in a Proterozoic minette dyke, Grenville province, Quebec. *Contributions to Mineralogy and Petrology* **125**, 319–331.

Nixon, P. H. (1987). *Mantle Xenoliths*. Chichester: John Wiley.

Nixon, P. H. & Boyd, F. R. (1973). Petrogenesis of the granular and sheared ultrabasic nodule suite in kimberlite. In: Nixon, P. H. (ed.) *Lesotho Kimberlites*. Maseru: Lesotho National Development Corporation, pp. 48–56.

Nowell, G. M., Pearson, D. G., Kempton, P. D., Noble, S. R. & Smith, C. B. (1999). Origins of kimberlites: a Hf isotope perspective. In: Gurney, J. J., Gurney, J. L., Pascoe, M. D. & Richardson, S. H. (eds) *The P. H. Nixon Volume, Proceedings of the 7th International Kimberlite Conference*. Cape Town: Red Roof Design, pp. 616–624.

Pearson, D. G., Canil, D. & Shirey, S. B. (2003). Mantle samples included in volcanic rocks: xenoliths and diamonds. In: Carlson, R. W. (ed.) *Treatise on Geochemistry, Vol. 2. The Mantle and the Core*. Amsterdam: Elsevier.

Pollard, D. D. (1987). Elementary fracture mechanics applied to the structural interpretation of dykes. *Geological Association of Canada Special Papers* **34**, 5–24.

Rabinowicz, M. & Ceuleneer, G. (2005). The effect of sloped isotherms on melt migration in the shallow mantle: a physical and numerical model based on observations in the Oman ophiolite. *Earth and Planetary Science Letters* **229**, 231–246.

Rabinowicz, M., Lago, B. & Froideveaux, C. (1980). Thermal transfer between the continental asthenosphere and the oceanic subducting lithosphere, its effect on subcontinental convection. *Journal of Geophysical Research* **85**(B4), 1839–1853.

Rabinowicz, M., Nicolas, A. & Vigneresse, J.-L. (1984). A rolling mill effect in asthenosphere beneath oceanic spreading centers. *Earth and Planetary Science Letters* **67**, 7–108.

Rabinowicz, M., Ricard, Y. & Grégoire, M. (2002). Compaction in a mantle with a very small melt concentration: implications for the generation of carbonatitic and carbonate-bearing high alkaline mafic melt impregnations. *Earth and Planetary Science Letters* **203**, 205–220.

Ribe, N. M. (1985). The deformation and compaction of partially molten zones. *Geophysical Journal of the Royal Astronomical Society* **83**, 487–501.

Ridgen, S. M., Ahrens, T. J. & Stolper, E. M. (1984). Densities of liquid silicates at high pressures. *Science* **236**, 1071–1074.

Ringwood, A. E., Kesson, S. E., Hibberson, R. W. & Ware, N. (1992). Origin of kimberlites and related magmas. *Earth and Planetary Science Letters* **113**, 521–538.

Rubin, A. M. (1993). Tensile fracture of rocks at high confining pressure: implications for dike propagation. *Journal of Geophysical Research* **98**, 15919–15935.

Rubin, A. M. (1995). Propagation of magma-filled cracks. *Annual Review of Earth and Planetary Sciences* **23**, 287–336.

Rubin, A. M. (1998). Dike ascent in partially molten rock. *Journal of Geophysical Research* **103**, 20901–20919.

Rudnick, R. L., McDonough, W. F. & Chappell, B. W. (1993). Carbonatite metasomatism in the northern Tanzanian mantle: petrographic and geochemical characteristics. *Earth and Planetary Science Letters* **114**, 463–475.

Sabadini, R. & Peltier, W. R. (1981). Pleistocene deglaciation and the Earth's rotation: implications for mantle viscosity. *Geophysical Journal of the Royal Astronomical Society* **66**, 552–578.

Scarfe, C. M., Mysen, B. O. & Virgo, D. (1987). Pressure dependence of the viscosity of silicate melts. In: Mysen, B. O. (ed.) *Magmatic Processes: Physicochemical Principles. Geochemical Society Special Publications* **1**, 59–67.

Scott, D. R. & Stevenson, D. J. (1984). Magma solitons. *Geophysical Research Letters* **11**, 1161–1164.

Scott, D. R. & Stevenson, D. J. (1986). Magma ascent by porous flow. *Journal of Geophysical Research* **91**, 9283–9296.

Skinner, E. M. W. (1989). Contrasting Group I and Group II kimberlite petrology: towards a genetic model for kimberlites. In: Ross, J. (ed.) *Kimberlites and Related Rocks, Vol. 1, Proceedings of the 4th International Kimberlite Conference*. Perth: Geological Society of Australia, pp. 528–544.

Sleep, N. H. (1974). Segregation of magma from a mostly crystalline mush. *Geological Society of America Bulletin* **85**, 1225–1232.

Sleep, N. H. (1988). Tapping of melt by veins and dykes. *Journal of Geophysical Research* **93**, 10255–10272.

Sleep, N. H. (2003). Geodynamic implications of xenolith geotherms. *Geochemistry, Geophysics, Geosystems* **4**, doi:10.1029/2003GC000511.

Smith, D. & Boyd, F. R. (1992). Compositional zonation in garnets of peridotite xenoliths. *Contributions to Mineralogy and Petrology* **112**, 134–147.

Smith, C. B., Gurney, J. J., Skinner, E. M. W., Clement, C. R. & Ebrahim, N. (1985). Geochemical character of southern African kimberlites: a new approach based on isotopic constraints. *Transactions of the Geological Society of South Africa* **88**, 267–280.

Sparks, D. W. & Parmentier, E. M. (1991). Melt extraction in the mantle beneath spreading centers. *Earth and Planetary Science Letters* **105**, 368–377.

Spera, F. J. (1984). Carbon dioxide in petrogenesis III: role of volatiles in the ascent of alkaline magma with special reference to xenolith-bearing mafic lavas. *Contributions to Mineralogy and Petrology* **88**, 217–232.

Spera, F. J. (1987). Dynamics of translithospheric migration of metasomatic fluid and alkaline magma. In: Menzies, M. & Hawkesworth, C. J. (eds) *Mantle Metasomatism*. London: Academic Press, pp. 1–19.

Spiegelman, M. & Kelemen, P. B. (2003). Extreme chemical variability as a consequence of channelized melt transport. *Geochemistry, Geophysics, Geosystems* **4**(7), 1055, doi:10.1029/2002GC000336.

Stevenson, D. J. (1989). Spontaneous small scale melt segregation in partial melts undergoing deformation. *Geophysical Research Letters* **16**, 1067–1070.

Stolper, E., Walker, D., Hager, B. H. & Hays, J. F. (1980). Melt segregation from partially molten source regions: the importance of melt density and source region size. *Journal of Geophysical Research* **86**, 6261–6271.

Sweeney, R. J. & Winter, F. (1999). Kimberlite as high-pressure melts: the determination of segregation depth from major-element chemistry. In: Gurney, J. J., Gurney, J. L., Pascoe, M. D. & Richardson, S. H. (eds) *The P. H. Nixon Volume, Proceedings of the 7th International Kimberlite Conference*. Cape Town: Red Roof Design, pp. 846–651.

Sweeney, R. J., Thompson, A. B. & Ulmer, P. (1993). Phase relations of a natural MARID composition and implication for MARID genesis, lithospheric melting and mantle metasomatism. *Contributions to Mineralogy and Petrology* **115**, 225–241.

Van Achterbergh, E., Griffin, W. L. & Stiefenhofer, J. (2001). Metasomatism in mantle xenoliths from the Letlhakane kimberlites: estimation of element fluxes. *Contributions to Mineralogy and Petrology* **141**, 397–414.

Van Thienen, P., van den Berg, A. P., de Smet, J. H., van Hunen, J. & Drury, M. R. (2003). Interaction between small-scale mantle diapirs and a continental root. *Geochemistry, Geophysics, Geosystems* **4**, doi: 10.1029/2002GC000338.

Watson, E. B., Brenan, J. M. & Baker, D. R. (1990). Distribution of fluids in the continental lithospheric mantle. In: Menzies, M. A. (ed.) *The Continental Lithospheric Mantle*. Oxford: Clarendon Press, pp. 111–125.

White, S. H., De Boorder, H. & Smith, C. B. (1995). Structural control of kimberlite and lamproite emplacement. *Journal of Geochemical Exploration* **53**, 245–264.

Wiggins, C. & Spiegelman, M. (1995). Magma migration and magmatic solitary waves in 3-D. *Geophysical Research Letters* **22**, 1289–1292.

Yaxley, G. M., Green, D. H. & Kamenetsky, V. (1998). Carbonatite metasomatism in the southeastern Australian lithosphere. *Journal of Petrology* **39**, 1917–1930.

Zoback, M. L. & Mooney, W. D. (2003). Lithospheric buoyancy and continental intraplate stresses. *International Geology Review* **45**, 95–118.